Determination of Spitzer Space Telescope focus from IRAC images without a focus slew

William F. Hoffmann[*a], Joseph L. Hora[b], J. Eric Mentzell[c], Catherine Trout Marx[c], Peter R. Eisenhardt[d], Sean J. Carey[e], S. Thomas Megeath[b], and John P. Schwenker[f]

[a]Steward Observatory, Univ. of Arizona, [b]Harvard-Smithsonian Center for Astrophysics
[c]NASA Goddard Space Flight Center, [d]Jet Propulsion Lab, [e]Spitzer Science Center,
[f]Ball Aerospace and Technologies Corp.

ABSTRACT

Prior to launch, the Spitzer Space Telescope (SST) secondary focus mechanism was set to a predicted desired in-orbit focus value. This predicted setting, determined from double-pass cold chamber measurements and calculated ground-to-orbit corrections, had an uncertainty greater than the required in-orbit focus accuracy. Because of concern about the potential for failure in a cryogenic mechanism affecting all Spitzer instruments, it was required that any focus correction be made in a set of moves directly from the initial to the desired setting. The task of determining the required focus moves fell to IRAC (Infrared Array Camera), the instrument most affected by and sensitive to defocus. To determine the focus directly from examining images at a fixed focus, we developed two methods, "Simfit" and "Focus Diversity" (W. F. Hoffmann, *et. al.*[1]). Simfit finds the focus by obtaining the best match between observed images and families of simulated images at a range of focus settings. Focus Diversity utilizes the focal plane curvature to find the best fit of the varied image blur over the focal plane to a model defocus curve. Observations of a single star at many field locations in each of the four IRAC bands were analyzed before and during the refocus activity. The resulting refocus moves brought the focus close to the specified requirement of within 0.3 mm from the desired IRAC optimum focus. This is less than a "Diffraction Focus Unit" ($\lambda \times (f/^2)$) of 0.52 mm at the SST focus at the shortest IRAC band (3.58 microns). The improvement in focus is apparent in both the appearance and the calculated noise-pixels of star images.

Keywords: simfit, focus diversity, telescope focus, simulated images, optical models, infrared, cryogenic, SIRTF, Spitzer Space Telescope, IRAC

1. INTRODUCTION

The Spitzer Space Telescope (SST), is an 85 cm f/12 Richey-Cretien all-beryllium telescope specified to be diffraction limited at a wavelength of 6.5 μm at its operating temperature of 5.5 K[2,3]. Three science instruments sharing the focal plane provide imaging from 3 to 180 μm and spectroscopy from 5 to 40 μm. IRAC (Infrared Array Camera) is an imaging instrument with four arrays sharing the focal plane in pairs. The nearly overlapping pass-bands are centered at 3.58, 4.52, 5.72, and 7.90 μm. Refractive optics provide diffraction limited images for the camera in all four bands. Each array has 256 x 256 pixels with a pixel scale of 1.22 arc-seconds. A result of this pixel scale is that the a point-source image is under sampled in bands 1 and 2 for which λ/D equals 0.7 and 0.9 pixels, respectively. Also, the image quality for bands 1 and 2 is limited by telescope aberrations in addition to diffraction. The IRAC instrument and its operation are described in detail in Hora *et. al.*[4], Fazio *et. al.*[5], and Lacy *et. al.*[6].

Prior to launch, the secondary focus mechanism was set to a predicted desired in-orbit focus value. While it had been hoped that the telescope would be in focus when it cooled to operating temperature in orbit, the predicted setting, determined from double-pass cold chamber measurements and calculated ground-to-orbit corrections, had an uncertainty greater than the required in-orbit focus accuracy, making refocusing the telescope in orbit a likely activity. Early in the SST program, the program management, wishing to minimize the likelihood or impact of a failure of the cryogenic secondary focus mechanism, set the rule that a focus slew could not be used to determine best focus. Instead the telescope focus must be determined some other way and then any required refocus be accomplished by moving directly from the initial to the desired focus setting. The resulting criterion and strategy for SST refocus is described in

[1*] whoffmann@as.arizona.edu, phone 520 621-6529, fax 520 621-1532, Steward Observatory, U of Arizona, Tucson, AZ 85721

Gehrz, *et. al.*[7] . Since IRAC is the instrument most affected by and sensitive to defocus, this task fell largely to the IRAC instrument and team.

In 1998, in response to the no focus-slew requirement, we suggested that focus determination could be accomplished by comparing in-orbit IRAC images of a star to simulated images generated from an optical model of IRAC and the telescope for a variety of model focus settings. The telescope focus would then be taken to be the model focus which provided the best match between the observed and simulated images. Initially this was met with some skepticism whether it would be sufficiently accurate, particularly near best focus and, in particular, whether there would be ambiguity which side of best focus the telescope was on. Simulations carried out with simulated images from an early telescope model, the image program IRAF (Image Reduction and Analysis Facility), and the Microsoft spread-sheet Excel, showed promise and encouraged us to begin what turned out to be a four year effort of development and testing. This led to the creation of two new techniques, "Simfit" and "Focus Diversity" and utilizing much of the capability of the Mathsoft Engineering & Education, Inc. program, Mathcad, to accurately and quickly process hundreds of star images semi-automatically to produce reliable focus determinations. It also required an extensive effort to produce and verify a sufficiently accurate optical model for creating the simulated images. The result is a remarkable focus determination accuracy of less than 0.2 μm focus motion at the secondary, equivalent to 0.02 mm at the telescope focal plane, and a successful refocus of the SST telescope. The achieved accuracy is just 1/25 of a diffraction focal depth ($\lambda \times f/^2$) for the shortest IRAC band.

The remainder of this paper describes the optical model, the two focus determination methods, and the successful focus determination and refocus of the Spitzer telescope in orbit. Much of the discussion of the optical models and the focus determination methods comes from Hoffmann *et. al.*[1]

2. SST/IRAC OPTICAL MODEL AND SIMULATED IMAGES

2.1. Creation of Models and Simulated Images Before Launch

The simfit and focus diversity methods depend on creation of satisfactory simulated images from an optical model that faithfully represents the system. Both the SST telescope and IRAC models were created in the Optical Research Associates ray-trace program, CodeV. The wavefront deformations, properties, and positions of the optical elements in the model were taken from measurements of individual components and subassemblies obtained at the operating temperatures. The IRAC component properties include variation with wavelength. The model was verified and refined by comparing model images to measured images obtained during end-to-end tests at Ball Aerospace and Technologies Corporation using their largest thermal vacuum chamber, known as the "Brutus" chamber[8,9]. For this purpose, the model for the SST telescope in orbit had to be altered for additional components, with their wavefront deformations where known to be significant. These are the changed geometry in the test chamber configuration, a distorted auto-collimation flat, a cryostat window, an extended "point source" located off-axis and in front of the in-orbit location of the focal plane, and the presence of gravity.

The model for the test chamber configuration was refined using the method of "phase retrieval"[9,10]. With this method, analysis of highly out-of-focus IRAC images were used to determine the wavefront error of the optical system. The difference between this wavefront error and that generated from the test chamber optical model was then used to refine the chamber optical model. Since it could not be determined how much of this difference came from the telescope and how much from items unique to the test chamber, such as the auto-collimating flat, there was some ambiguity about how much, if any, of this correction should be applied to the in-orbit model. As discussed in section 2.2, the weighting for this correction was determined by optimization in orbit.

Given the model, simulated images for each IRAC band are created by ray tracing allowing for varying spectral response and for diffraction. This is done in the following steps.

1. Create a set of rays from a point source at infinity to the focal plane array, uniformly covering the SST aperture and sampling the wavelength range of the array. This is done for a particular telescope secondary focus setting and position on the array. For measuring the focus in orbit, we have chosen a square grid of 25 positions in each field-of-view to provide reasonable spatial sampling. The coordinates of these positions in pixels in each axis are 24, 76, 128, 180, and 232. The focus settings range from –50 to +50 μm in steps of 2.5 μm at the secondary focus mechanism.

2. Use the ray-trace data to compute the wavefront aberration of the system. Then by Fast Fourier Transform, compute the diffraction image distribution at the plane of the array for each wavelength sampled.
3. Sum these intensity distributions over wavelength, weighting for the spectral response of the array and filter and for the source spectrum (Rayleigh-Jeans for a star).
4. Bin the summed wavelength intensity data into a grid of sub-pixels each one-fifth the size of an IRAC pixel. This grid is centered on the source and has the same number of sub-pixels as IRAC pixels on the array.
5. Format the results as a FITS image file. For the given model a total of 4100 images are created for the 25 field positions, 41 focus settings, and four IRAC bands.

2.2. Refinement of the Model with Analysis of In-Orbit Images

Because of uncertainties in the differences between the test chamber and in-orbit optical configuration, there was concern about how well the in-orbit model inferred from the test chamber results would apply in space. Three items of particular concern were

1. The appropriate fraction of the phase retrieval correction determined for the test chamber configuration that should be applied to the in-orbit model
2. Difference in the secondary decenter in orbit from that chosen from the pre-launch measurements. A number of geometric measurements of the decenter carried out at Ball Aerospace and Technologies Corp. before and after cool-down and after shipping to Lockheed Martin Space Systems Co. and to Kennedy Space Flight Center showed shifts in decenter ranging over 0.044 mm in both the z and y directions.

In order to prepare for these uncertainties, a full set of simulated images were prepared for 10 different models, five with the phase retrieval wavefront correction and five without. The five models were for a square array of z and y decenters centered on the most likely prediction. With 4100 images per model, a total of 41000 simulated images were created and used in the in-orbit analysis. In addition, the simfit and focus diversity analysis programs had the capability of adjusting the charge diffusion blur characteristic of the InSb arrays in Bands 1 and 2, adding any other source of Gaussian blurring, and altering the pixel scale, image rotation, and background level.

Optimization for these parameters was carried out by analyzing images early in the In-Orbit Checkout (IOC) IRAC focus campaigns with a variety of sets of values for the parameters. Best values for the parameters were determined by interpolating the models to give the best correlation between the simulated and observed images. Optimizing for phase retrieval correction, secondary decenter, and for Gaussian blur improved the fit considerably. Varying the other parameters had little affect on the fit quality. Table 1 shows the initial and optimized parameter values. The optimized values were used for the analysis in this paper. It is remarkable that the secondary decenter of the telescope can be determined to a few μm by just examining a few images in orbit.

If the model and telescope focal plane shape at the detector (tilt and curvature) and focus offsets between bands are the same for the model and the in-orbit system, the secondary focus setting determination should have the same value for each of the 25 field positions and four arrays. Systematic differences in focus for different field positions and bands repeating from one focus campaign to another indicate errors in the model for focal plane shape and offset. Such differences were found. Correcting for them resulting in. a reduction of scatter in the simfit and focus diversity results

3. METHODS: SIMFIT AND FOCUS DIVERSITY

3.1 Simfit Concept

Underlying Simfit is the fact that as an instrument or telescope is defocused, the image of a point source not only becomes larger, but also changes its shape due to changing ray paths through the system and the effects of pupil location, obscuration, optical aberrations, and diffraction. These changes are different on the two sides of best focus. This is true even very close to best focus. By comparing an observed image with a family of simulated images and determining which simulated image fits most closely to the observed image, we can uniquely determine the telescope focus setting for the observed image, hence both the distance and director of defocus. We have used two different algorithms for the image comparison, cross correlation and blink. Cross correlation is a multiplicative comparison. Blink is a subtractive comparison. The name, blink, is derived from the classical method for discerning a small motion

or brightness change of a source in a star field by alternately viewing (blinking) two images. The algorithms are given in Equations 1 and 2 where *Star* is the observed source, *Simin* is a member of the family of simulated images, and *i* and *j* are indices for the rows and columns of a portion of the array covering the source.

$$Crosscor = \frac{\sum_{i,j} Star_{ij} \times Simim_{ij}}{\sqrt{\left(\sum_{i,j} \left(Star_{ij}\right)^2 \times \sum_{i,j} \left(Simim_{ij}\right)^2\right)}} \quad (1)$$

$$Blink = 1 - 0.5 \times \sum_{i,j} \left| \frac{Star_{ij}}{\sum_{i,j} Star_{ij}} - \frac{Simim_{ij}}{\sum_{i,j} Simim_{ij}} \right| \quad (2)$$

Table 1. Model Corrections from Image Analysis During IOC

This table gives the initial and optimized values of the telescope secondary z and y decenter (in Ball Aerospace Cryogenic Telescope Assembly (CTA) coordinates, the optimal fraction of phase retrieval wavefront correction, the charge diffusion Gaussian blur for Bands 1 and 2, and additional Gaussian blur for Bands 3 and 4. These corrected values were used for generating the simulated images used in the analysis reported in this paper. They result in a considerably better fit between the observed and simulated images than the images generated with the initial values. The phase retrieval correction tends to sharpen images as does a smaller Gaussian blur. Hence, the images for Bands 1 and 2 are somewhat sharper than expected and those for Bands 3 and 4 less sharp.

IRAC Band		1	2	3	4
Telescope Corrections					
z-secondary decenter (mm)	Initial	-0.013			
	Corrected	+0.004			
y-secondary decenter (mm)	Initial	-0.060			
	Corrected	-0.049			
Phase retrieval correction (fraction)	Initial	0			
	Corrected	0.75			
Image Blur					
Telescope jitter (FWHM pixels) (0.1 arcsec sigma)	Initial	0.14			
	Corrected	0.14			
Array charge diffusion (FWHM pixels)	Initial	0.47	0.47	0	0
	Corrected	0.40	0.35	0	0
Required additional blur diffusion (FWHM pixels)	Initial	0	0	0	0
	Corrected	0	0	0.64	0.33
Total image blur (FWHM pixels)	Initial	0.49	0.49	0.14	0.14
	Corrected	0.43	0.37	0.65	0.36

Both algorithms result in a single number for the quality of the fit that is 1 for a perfect fit and 0 for no overlap of the images. Both require the zero flux level to be accurately established. Both require that the simulated images be precisely registered to the position of the observed image relative to a pixel center. That is, the centroids of the observed and simulated images must be identical. It is desirable that the comparison be carried out over a portion of the array centered on the source and containing at least 90% of the source flux. We have generally used the blink algorithm, which provides greater sensitivity near best focus.

3.2 Initial Image File Processing

The program which carries out the Simfit calculations from reading observed and simulated image files to displaying graphically and numerically the results is Mathcad 2001 Professional operating under Microsoft Windows 2000 Professional. Mathcad provides ample array and imaging processing and image display capability. Its "you see what you get" format is convenient for a non-programmer and for documentation. The following steps are for initial imaging processing used for both simfit and focus diversity.

1. Transfer the IRAC pipeline processed image files for the current IRAC focus campaign from an IRAC computer to the simfit computer.
2. For a selected IRAC band, read the files of the star images obtained for all dithered positions at the 25 field locations. The definition of these locations is given in Section 2.1, step 1.
3. Locate the position of the brightest star in each image by row and column. This is done with a median 2×2 box filter which suppresses artifacts affecting only one or two pixels. Determine the closest of the standard 15 field positions. Crop images to the desired box size (7×7 pixels).
4. Compute for each image the row and column centroids, total flux, peak and minimum pixel flux, and noise-pixels (defined in Section 3.4)
5. Mark as rejected any image too close to the array edge or with the total flux, peak and minimum flux, peak-to-total flux, or noise-pixels out of range.
6. Select images to be analyzed from the non-rejected images. These can be all the remaining dithered images or one for each field position selected as the one with the minimum, maximum, or median NP, minimum centroid, or maximum peak flux. The focus determination value was largely independent of this choice of images.
7. For each selected observed image, read the set of sub-pixel simulated image files for the same band and nearest field location covering a range of telescope focus setting. These are at a 2.5 μm secondary focus spacing.
8. Blur the simulated images for all bands for telescope jitter, for Bands 1 and 2 charge diffusion, and for Bands 3 and 4 additional blur.
9. For each blurred simulated image combine the sub-pixels into IRAC sized pixels over the chosen analysis box size, shifting to provide the same centroid as the corresponding star image. The shifting is done to fractional sub-pixels by 16-point bi-quadratic interpolation. The process is iterated until the centroids agree to within 0.01 pixels

3.3 The Simfit Process

The additional steps for the simfit process are:

1. Carry out the blink (or cross correlation) algorithm between the star and each of the simulated images. The result is a set of values of the Simfit parameter that peaks for the simulated image whose focus is closest to that of the star image.
2. Repeat Sect 3.2 steps 6 and 7 and Sect 3.3 step 1 using a set of simulated images with closer focus spacing obtained by interpolation from the initial set.
3. Interpolate the fine-focus results to obtain the focus setting for the best-fitting image to a fraction of a μm at the secondary.

Figure 1 provides an illustration for these steps with the simfit analysis of a single observed Band 1 image from Campaign M at the edge of the field. The process for all selected images for the 25 focal plane positions is carried out automatically. For the case of randomly located stars (Campaigns A, B, R-T) the process is carried out by interpolating the simulated images and best-focus difference from the nearest standard field positions to the location of the star. The program provides a simfit plot for all the analyzed images and a focus determination taken to be the median of the individual results. Since the four IRAC bands are not exactly con-focal, the focus determination for a campaign is taken to be the mean of the focus values for bands 1 and 2 which are the bands most sensitive to focus.

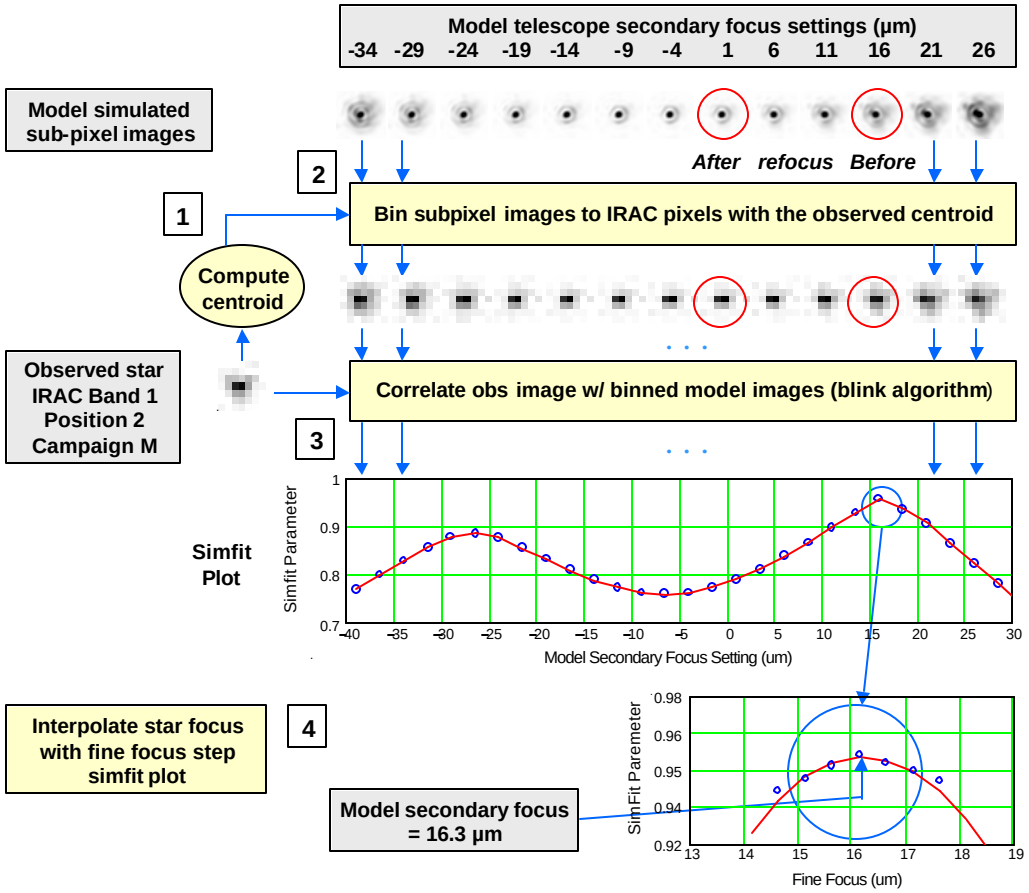

Figure 1. Simfit focus determination method demonstrated with an IRAC Band 1 observed star. A cropped image of an IRAC Campaign M Band 1 observed star is shown in the center left of the figure. This star was chosen from the set of dithered images at position 2 in the focal plane as defined in Figure 2. At the top of the figure is a set of sub-pixel simulated images for the same IRAC band and the same field position as the observed star. The images are produced from an optical model with a pixel resolution five times that of IRAC and secondary focus settings separated by 2.5 μm, with every other one shown in this figure. The sub-pixel model images show clearly diffraction rings, structure from telescope aberrations, and the trifoil shape attributed to the secondary mirror support. The circled images are at focus settings close to those before and after refocus of the telescope. In Step 1, the centroid of the observed star image is calculated relative to a pixel center. In Step 2, the simulated images are each binned into IRAC sized pixels with exactly the same centroid as the observed image. The observed and binned images show the IRAC Band 1 under-sampling of the Airy disk with one pixel equaling 0.71 λ/D. In Step 3, the binned simulated images are correlated with the observed image to give values which are 1.0 for a perfect correspondence and 0.0 for no overlap. The resulting correlations plotted versus the secondary settings for the simulated images show two peaks on opposite sides of best focus. The simfit focus determination is the focus value at the higher peak. Step 4 repeats the simfit plot for simulated images with closer focus spacing near the peak. The final focus determination is obtained from the maximum of a quadratic curve best fit to the points. The result for the analysis of this image is 16.3 μm. Repeating the analysis for the images over a grid of 25 positions on the array with dither allows averaging out systematic errors. The standard deviation for this result over several IRAC campaigns is 0.14 μm.

3.4 Focus Diversity

Focus diversity depends on the variation in the defocus blur of images over a field due to focal plane curvature and tilt. This would normally be considered to be a weakness of the design or assembly of an instrument. However, the presence of focus diversity can be used to accurately determine the focus of a system relative to an optimum focus with images obtained at only one focus setting of the system. This is the same objective as that given for the simfit method. The procedures and requirements of the two methods are very different. As a consequence, these two methods are complementary and provide an excellent check on each other. Two of the major differences are:

1. Focus Diversity and Simfit both require an optical model but for very different reasons. Simfit requires the model to produce simulated images that are accurately matched to the observed image in order to select the focus setting from the best matching simulated image. Focus diversity requires the model to determine the image blur and best focus setting for best focus at each selected position in the field and a defocus blur curve.
2. Simfit can, in principle, determine the telescope focus from a single star image at one field location. Focus Diversity requires a set of images obtained at different positions in the field.
3. Simfit provides a focus determination but no particular information about the image quality or blur. Focus diversity clearly presents any degradation from defocus image blur.

Essential to the focus diversity method is a suitable measure of image blur caused by defocus. This measure must not be seriously degraded by image under-sampling or noise. For this we have chosen noise-pixels (NP)[11]. NP are the equivalent number of pixels for calculating the random noise when an image is spatially filtered for optimum faint point-source detection. The optimum filter is directly related to the point-spread-function of the system. The equivalent number of NP is given in Equation 3. *Star* can be the instrument point-spread-function or a high signal-to-noise image of a point source. *i* and *j* are indices for the rows and columns of a portion of the array covering the source. If the star flux is equally distributed over one or more pixels, NP equal the number of pixels covered by the star. The more concentrated the image of a star, the smaller the number of NP.

$$\text{noise-pixels} = \frac{\left(\sum_{i,j} Star_{ij}\right)^2}{\sum_{i,j} \left(Star_{ij}\right)^2} \tag{3}$$

NP are directly related to a number of more familiar concepts. Integration time for faint source detection at a given sensitivity increases linearly with NP. The sensitivity for a fixed integration time is proportional to the square root of NP. The inverse of NP, called "sharpness", is a measure of image concentration. NP can be thought of as a measure of the extent, or blur of an image of a point source. The diameter of a point source is proportional to the square root of NP

The calculation of NP is somewhat sensitive to pixel phase (location of source peak or centroid relative to a pixel center). For comparison of NP from one position to another in the field or from one IRAC band to another we use normalized NP. This is the ratio of the measured NP to NP of a simulated image at best focus for the same pixel phase, band, and position on the field. This accounts for differences in NP at best focus over the field and for different bands due to increased image size from diffraction.

As with other measures of defocus, such as full-width-half-maximum, when an instrument is scanned over a focus range, NP for a point source reach a minimum at best focus and increase on either side of best focus. For an image that is structured due to aberrations, the best-focus setting will be slightly different for different measures of image blurring. The best focus determined by NP gives the best point source signal-to-noise

The steps for Focus Diversity are given in Figure 2. This figure shows as inputs, cropped observed images for a selection of the 25 positions on the field of IRAC Band 1 Campaign M, the best-focus setting and minimum NP from the simulated image for the selected positions, and the defocus curve used in the plots. The steps are to calculate NP, calculate the defocus variable for each position for a given focus setting, and plot the normalized NP versus defocus. In Figure 2, the latter two steps are carried out first with a focus setting of zero, to illustrate the procedure. For this focus setting, the points clearly do not lie on the line, since zero is far from the roughly 16 μm setting of the telescope. The second and third steps are then repeated with the focus setting determined by a least-square fit of the points to the defocus curve.

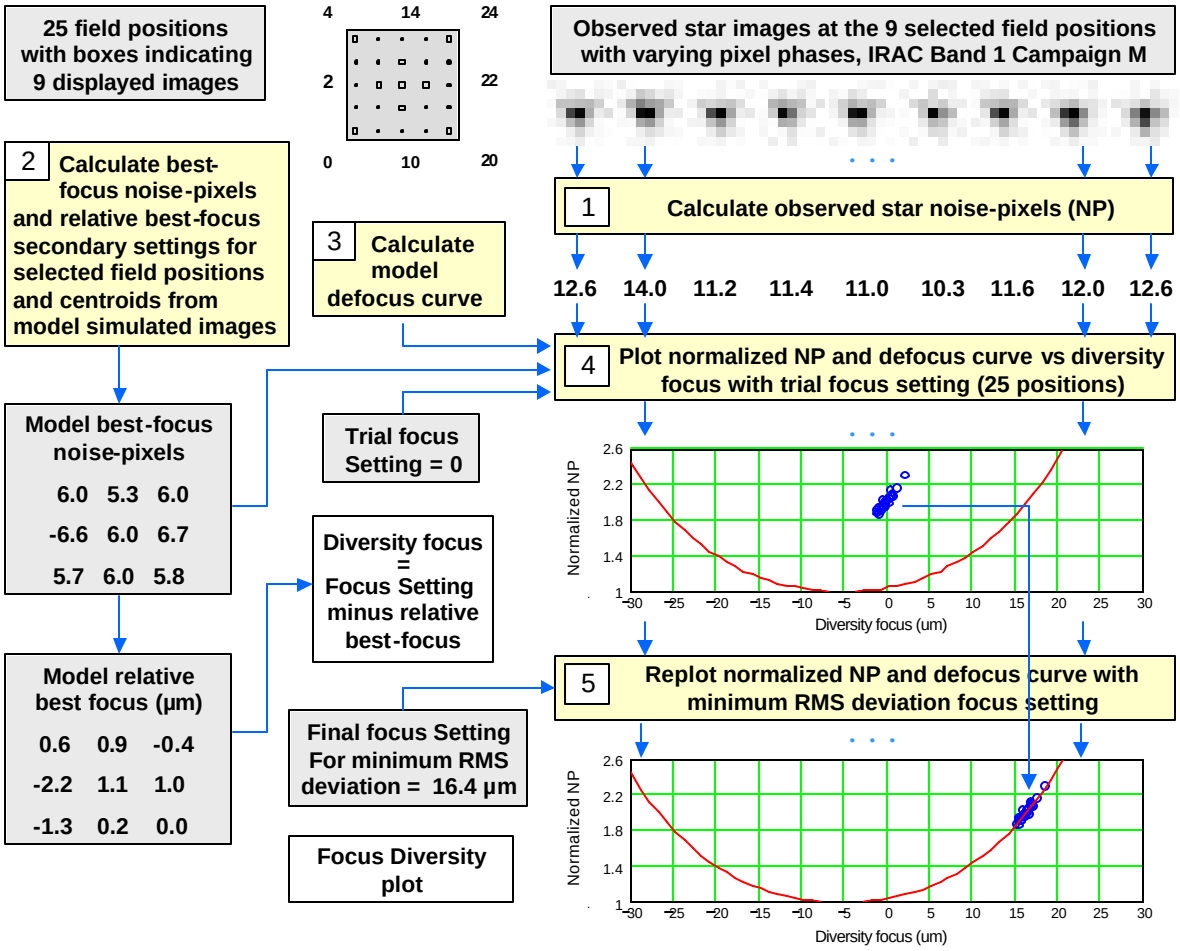

Figure 2. Focus Diversity method demonstrated with IRAC Band 1 observed star images. The focus diversity method takes advantage of relative image defocus due to the curvature and tilt of the focal plane. The square at the top of the figure shows the grid of 25 focal plane positions for which the star is observed. The open boxes indicate the positions of the nine IRAC Campaign M, Band 1, observed images displayed to the right. In Step 1 noise-pixels (NP) and centroids are calculated for each observed image. In Step 2 the model best focus NP and secondary settings are calculated from the model images for each of the 25 focal plane positions and observed image centroids. The values are shown for the nine displayed positions. The best focus secondary settings are given relative to the mean setting. In Step 3 a defocus curve is calculated from the model giving the normalized NP versus secondary focus setting. The curve has a minimum of 1.0 at the best focus for the mean of the focal plane positions for this band. In step 4 the star NP values are normalized by dividing by the value of NP at best-focus and these results plotted along with the defocus curve versus diversity focus with a trial focus setting of zero. Clearly the points do not fit the curve with this value. In Step 5 the focus setting is determined for which the standard deviation of the points from the curve is minimized. The defocus curve is slightly different for each field position and pixel phase. For determining the focus setting as the best rms fit for the observed NP the individual curves are used. For the purpose of the plot, the data points are shifted to compensate for these differences and fit a single curve. The resulting telescope secondary focus setting is 16.4 µm, very close to the 16.3 µm setting determined by the simfit method in Figure 1. This is far from the Band 1 model best focus which, from the defocus curve, is close to –6 µm. In principle, the secondary focus could be obtained from focus diversity with just one star image with uncertainty which side of best focus to choose. Using several focal plane positions with different relative defocus removes this uncertainty and provides reduced error.

4. FOCUS DETERMINATION RESULTS

4.1 Cool-down Focus Trend and Refocus Result

Running from the 8th to 50th day after launch twenty IRAC "Campaigns" were carried out obtaining images suitable for simfit and focus diversity analysis. Fifteen of them, Campaigns C through Q, were carried out for the grid of 25 field points specifically for focus determinations. Campaigns A, B, and R-T produced images of stars randomly over the field, which were still suitable for simfit analysis. For all these campaigns, a telescope focus setting, relative to the model zero setting, was determined as the average of the simfit values for Bands 1 and 2. The results are given in Figure 3. The horizontal axis is day from launch and the vertical axis the secondary setting in µm relative to the model zero. The dashed line is the optimum focus for which bands 1 and 2 have an equal excess of NP over the best focus value. The dot-dash lines give the +/- 3 µm acceptable range from optimum[7]. The filled circles are the focus determinations from each campaign. The campaign letters and telescope temperatures are at the bottom. The first focus measurement is negative and far from the others because of initial transient temperature differences in the telescope. By Campaign F, the focus values settled down to a value of 16.5 µm with a standard deviation of 0.14 µm. The result of the first (exploratory) move of –2 µm is clearly shown in the "O" determination and the second, major move of –13 µm in the P determination. Subsequently, the Q through T determinations settle down to a stable focus.

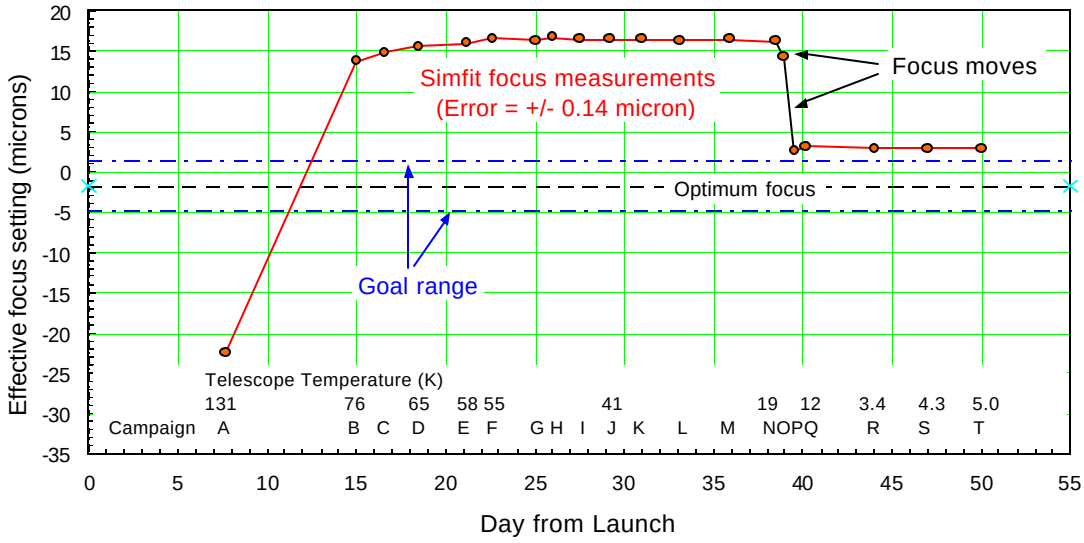

Figure 3. Simfit focus determinations during telescope cool-down and early orbit operation. The filled circles plot the effective telescope secondary focus settings relative to the model zero versus the day from launch. The IRAC Campaign letters and associated telescope temperatures are given at the bottom of the graph. The optimum focus of –1.8 µm and acceptable range of +/- 3.0 µm relative to this are shown as dashed and dash-dot lines. The focus settings are the average for IRAC bands 1 and 2 determined by the simfit method. For campaigns C through Q, each band result was determined from the images of a selected star on a grid of 25 positions on each focal plane with 4 dither settings per location, except for campaigns I, M, and Q which had 12 dither positions. For campaigns A, B, and R through T, the focus was determined from a relatively random set of stars on fields obtained for other tasks. The first focus measurement is negative because of transient temperature differences in the telescope. By the time the telescope reached a temperature of 55 K, the focus had settled to a value of 16.5 µm, which is 18.3 µm greater than the optimum focus determined before launch. At day 38 an initial "exploratory" move of -2 µm was made with 6 secondary focus stepper motor steps. This is clearly seen on the plot. On day 40, a main move of -13 µm was carried out. A planned third move of -4 µm was not made because of ambiguity in interpreting of the focus diversity results at the time. This left the focus setting slightly outside the acceptable band.

4.2 Simfit and Focus Diversity Plots Before and After Refocus

In each IRAC focus campaign a selected star is imaged at each of the 25 positions in each of the IRAC paired fields, that is the Band 1 – Band 3 and Band 2 – Band 4 fields. At each field position redundant images are taken at either 4 or 12 dithered positions. One of the dithers at each position is selected for processing so that there are 25 independent simfit focus determinations and one focus diversity determination. The overall focus result is taken to be the average of the medians of the simfit determinations for Bands 1 and 2. The focus diversity results are used for confirmation and to display the effect of defocus on the image blur.

Figures 4 and 5 show before (Campaign M) and after (Campaign Q) simfit and focus diversity plots for each IRAC band. The simfit plot is for one of the 25 positions. The focus diversity plot uses the results for all positions. The before simfit plots for Bands 1-3 each show the double hump with peaks on either side of best focus characteristic of an out-of-focus image. The Band 4 plot does not show the double hump because it is closer to best focus and has a greater depth of field. It does show asymmetry characteristic of imperfect focus. The before focus diversity plots for Bands 1-3 show the points for the 25 field positions high on the defocus curve indicating considerable image blur degradation. For Band 1 the mean NP is twice the value at best focus.

The after simfit plots all show improvement with all but Band 1 single peaked and nearly symmetrical. The Band 1 plot continues to show the secondary peak on the other side of best focus from the main peak. The focus diversity plots for Bands 2-4 show all the points below the 10% excess NP line (horizontal dashed line at a normalized noise pixel value of 1.1). The points for Band 1 are higher, but the mean is close to 1.1 meeting the refocus criterion established before launch[7]. If the third refocus move of -4 μ and complementarity of simfit and focus diversity with simfit providing an accurate measurement of the secondary focus setting, focus diversity showing the degraded image blur from defocus, and both plots indicating clearly how far the secondary must be moved to bring about optimum focus.

4.3 Point-spread-functions (PSF) and star images for the four IRAC bands before and after refocus

Figure 6 shows before and after refocus star images for the four IRAC bands. The upper two rows present point-spread-functions (PSF). Each PSF is constructed from 108 images, each observed with a slightly different telescope pointing (dither). The PSF's are created with a "drizzle" algorithm with sub-pixels 1/4 the size of the IRAC pixel. Bands 1 and 2 show clearly a reduction in the trifoil appearance after refocus. All four bands show greater flux concentration in the central core.

The next two rows show a single observed image from each IRAC band before (campaign M) and after (campaign Q) refocus. Each image is chosen from the 25 field positions and 12 dithers to have a median NP and to have the peak of the star nearly centered on a pixel. These images show the pixel under-sampling, in particular in Bands 1 and 2, but have a very similar appearance to the PSF images.

The bottom row shows model images for best focus in each band for the same field position and pixel centering as the observed images. These images show the close agreement in shape and structure between the observed and model images. The difference between the after refocus observed and best focus model images is marginally discernable visually, mainly with the Band 1 images.

4.4 Noise-pixels before and after refocus

Table 2 gives noise-pixels (NP) for the selected images shown in Figure 6. Each image was chosen from the 12 dither images at each field position to have NP near the median for the 12 and from the resulting set of images for the 25 field positions to have the most peaked image. Refocusing clearly reduced the NP for Bands 1-3 with nearly a factor of two reduction for Band 1. The after-refocus NP for Bands 2-4 are very close to the model best-focus NP for the same field position and pixel centering. The after-refocus NP for Band 1 is 15% above the best-focus NP, indicative of the residual defocus of that band. Interestingly, the final focus setting left Band 2 very near its best focus and the NP, hence image size, of the Band 1 image very similar to the Band 2 image size. This could be an advantage for some scientific investigations. The NP values given in Table 2 are lower than those given in Hora *et. al.*[3],and Gehrz *et. al.*[6] because their values are for the mean, rather than m had been carried out, the points for Bands 1 and 2 would have appeared symmetrically on opposite sides of the minimum NP with all points below the 1.1 line.

These plots show clearly the effectiveness a single chosen sharp image, and because they are computed over a larger number of pixels.

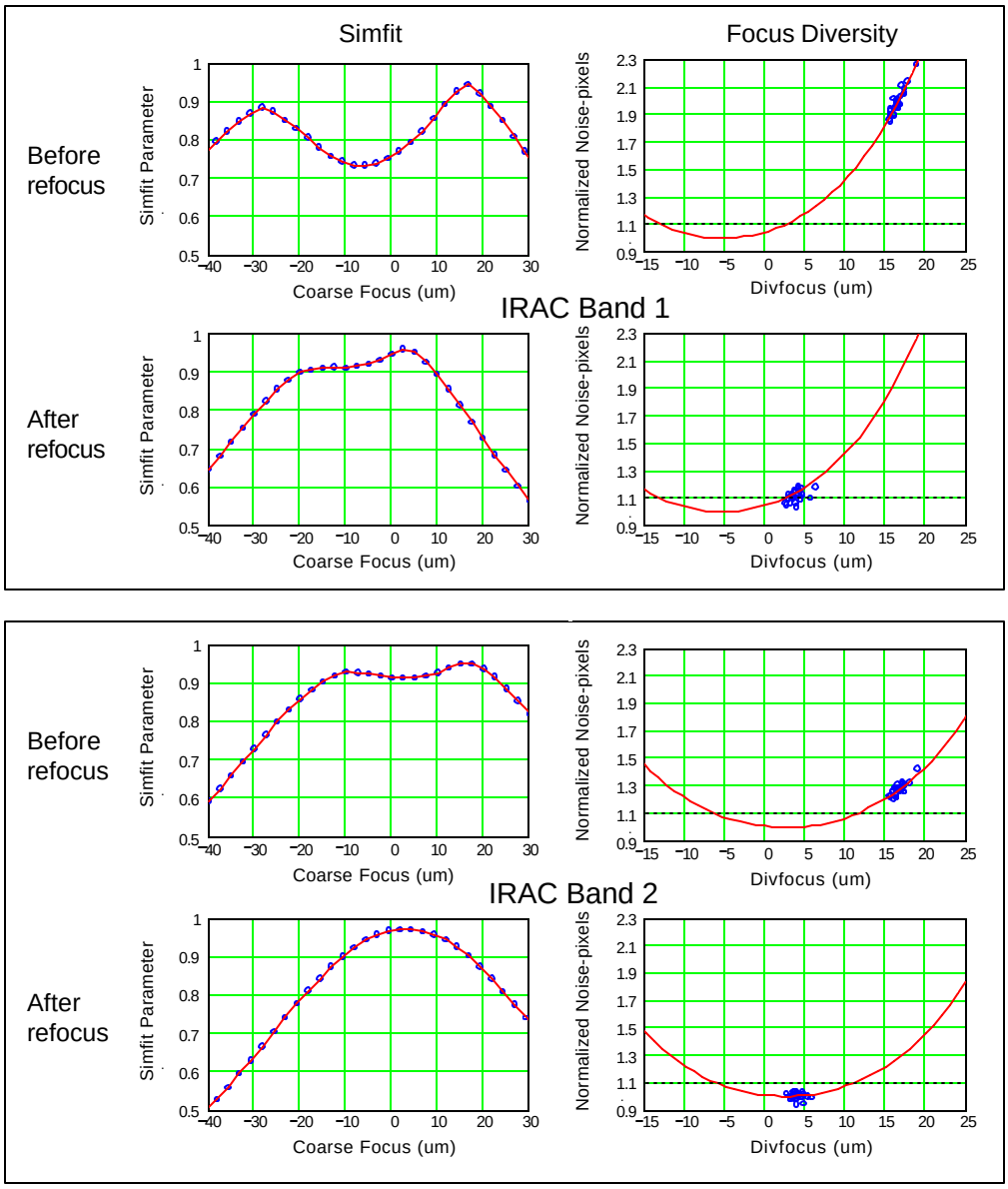

Figure 4. Simfit and Focus Diversity plots before and after refocus for IRAC bands 1 and 2. The simfit plots are shown for a single observed image at one of the 25 field positions and dithers from IRAC campaigns M and Q. The points with a line connecting them are the simfit parameter plotted against the telescope secondary focus setting in 2.5 μm steps. In the before-refocus plots there are two peaks roughly equally spaced on either side of best focus with the higher peak providing the focus setting for the best fit between the observed and simulated image. At best focus for the given band and focal plane position the simfit plot would be a single peaked symmetrical curve centered on best focus. The double hump in the band 1 after-focus plot indicates that band 1 remains on one side of best focus after refocus. The single peaked symmetrical curve in the band 2 refocus plot indicates that band 2 is very nearly at best focus.

The focus diversity plots show normalized noise pixels (NP) for one of the dithers for each of the 25 focal plane positions plotted against the secondary focus. The curve is the model defocus curve that has a minimum of 1.0 at best focus. The shift in the minimum of these curves between bands 1 and 2 from –5 to +3 μm is due to the non-confocality of their focal planes. The dashed line at 1.10 is the maximum mean normalized NP determined before launch to be acceptable. The optimum focus was defined to be the focus for which the mean normalized NP for Bands 1 and 2 are the same. The refocus activity did not quite reach this optimum focus, leaving both bands on the same side of best focus with Band 1 further from best focus and the mean Band 1 normalized NP just meeting the maximum acceptable value. The mean normalized NP for Band 2 after refocus is well below the requirement.

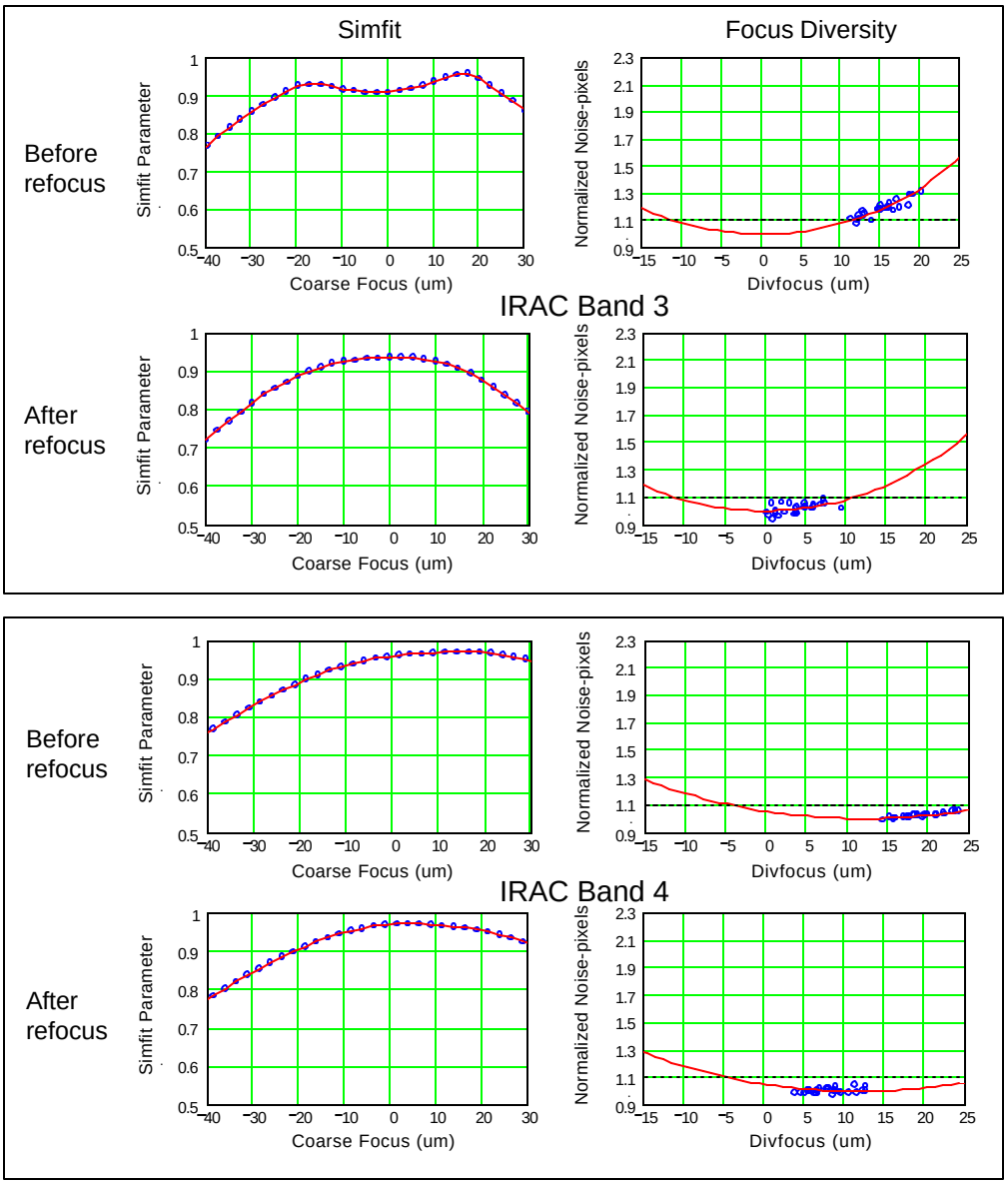

Figure 5. Simfit and Focus Diversity plots before and after refocus for IRAC bands 3 and 4. The simfit plots are shown for a single observed image at one of the 25 field positions and dithers from IRAC campaigns M and Q. The points with a line connecting them are the simfit parameter plotted against the telescope secondary focus setting in 2.5 μm steps. The curves are broader and less peaked than those for bands 1 and 2 because of the larger diffraction image size. In the before-refocus plot for band 3 there are two peaks roughly equally spaced on either side of best focus with the higher peak providing the focus setting for the best fit between the observed and simulated image. At best focus for the given band and focal plane position the simfit plot would be a single peaked symmetrical curve centered on best focus. After refocus, bands 3 and 4 show a relatively symmetrical single peaked curve indicating that they are near to best focus.

The focus diversity plots show normalized noise pixels (NP) for one of the dithers for each of the 25 focal plane positions plotted against the secondary focus. The curve is the model defocus curve that has a minimum of 1.0 at best focus. The shift in the defocus curves between bands 3 and 4 from +1 to +11 μm is due to the non-confocality of their focal planes. The curves for bands 3 and 4 are much broader and flatter than those of bands 1 and 2 because of the larger diffraction image size. The dashed line at 1.10 is the maximum mean normalized (NP) determined before launch to be acceptable. The mean normalized NP for bands 3 and 4 after refocus are well below this requirement.

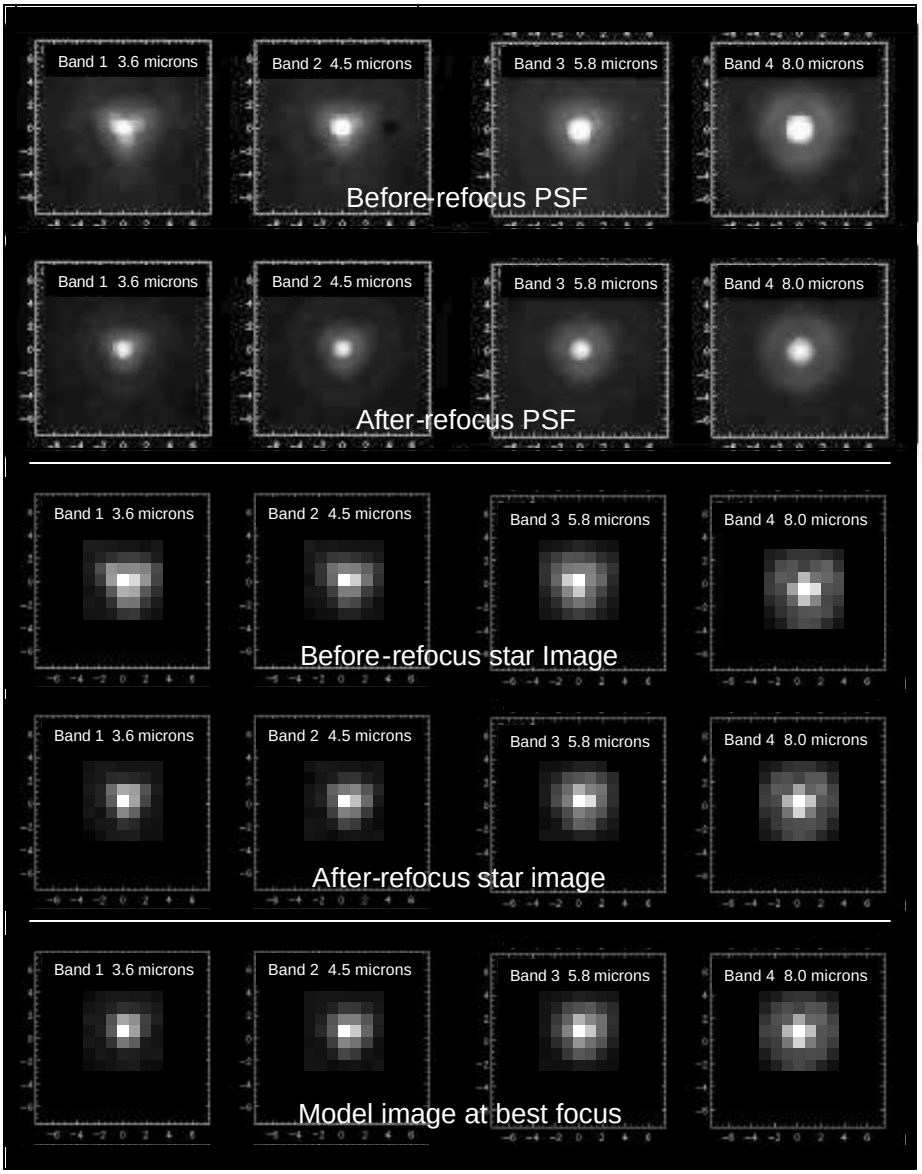

Figure 6. Point-spread-functions (PSF) and star images for the four IRAC bands before and after refocus The box size is 15 IRAC pixels (18.3 arc-seconds). The images are displayed with square root scaling to bring out the low level extended structure. In the upper two rows each PSF is constructed from 108 images, each observed with a slightly different telescope pointing (dither). The PSF's are created with a "drizzle" algorithm with sub-pixels 1/4 the size of the IRAC pixel (i.e. there are sixteen pixels for each IRAC pixel). Most of the flux is in the central core surrounded by the first Airy ring, as expected from diffraction. In bands 3 and 4, the first ring is clearly separated from the core with a fainter second ring barely visible. The bands 1 and 2 PSF's show a trifoil, or triangular, pattern attributed to the method of secondary mirror support. The improvement in PSF sharpness after refocus is clear in all four bands with the largest improvement in bands 1 and 2.

The 3rd and 4th rows show a single observed image from each IRAC band before (campaign M) and after (campaign Q) refocus. Each image is chosen from the 25 focal plane positions and 12 dithers to have a median NP and to have the peak of the star nearly centered on a pixel. These images show the undersampling of the PSF and the trifoil shape, particularly in bands 1 and 2. They also show clearly the improvement in image concentration after refocus.

The bottom row shows model images for best focus in each band for the same focal plane position and pixel centering as the observed images. These images show the close agreement in shape and structure between the observed and model images. The difference between the after-refocus observed and best-focus model images is marginally discernable visually, mainly with the band 1 images.

Table 2. Noise-pixels of selected images before and after refocus.

This table gives noise-pixels (NP) for the selected images used in Figure 6. Each image was chosen from the 12 dither images at each focal plane position to have NP near the median for the 12 and from the resulting set of images for the 25 focal plane positions to have the most peaked image. The NP for the before-focus images for all but band 4 were substantially blurred from defocus. The NP after refocus were close to the best-focus value for all except band 1. The normalized NP are the NP values divided by the model best-focus NP. The after-refocus normalized NP values show that bands 2-4 are all near the minimum (best-focus) value of 1.00 with band 1greater than this. Prior to SST launch the acceptable mean normalized NP was taken to be less than 1.10. The focus goal was a compromise between best focus for Bands 1 and 2 with the mean normalized NP of each about 1.03. The achieved focus favors Band 2 with Band 1 slightly above the acceptable value. The NP values in Hora *et. al.*[4],and Gehrz *et. al.*[7] are larger that those given here because they are for the mean, rather than a single chosen sharp image, and because they are computed over a larger number of pixels.

IRAC Band	1	2	3	4
	Noise-pixels			
Before Refocus	10.3	6.7	10.2	11.4
After Refocus	5.4	5.5	8.5	11.3
Model Best Focus	4.7	5.5	8.3	11.0
After Refocus Normalized	1.15	1.00	1.02	1.03

5. SUMMARY

The newly developed techniques of simfit and focus diversity and the SST/IRAC optical model created to support these techniques all met, or exceeded expectations. They made it possible for the focus of the SST telescope to be accurately monitored as the telescope cooled during In-Orbit Checkout, for the telescope to be confidently refocused on schedule, and for the observing consequences of the initial defocus and final refocus to be clearly displayed.

6. ACKNOWLEDGEMENTS

We thank the SST Focus Integrated Products Team (IPT), in particular, the co-chairs, Bob Gehrz and Ed Romana, for their encouragement, support, and critical discussions during the development of the simfit and focus diversity techniques. We also thank the SST project manager, Dave Gallagher, and project scientist, Mike Werner, and the SST instrument principal investigators Giovanni Fazio, George Rieke, and Jim Houck for their acceptance and advocacy of the importance of achieving the best possible image quality of the IRAC camera by optimal focusing, and their confidence in the simfit and focus diversity methods for achieving this. We appreciate the test team at Ball Aerospace for their cooperation taking the measurements during the cryogenic chamber telescope tests needed to validate and perfect these techniques.

7. REFERENCES

1. W.F. Hoffmann, J. L. Hora, J. E., Mentzell, C. T. Marx, P. R. Eisenhardt, "Simfit and Focus Diversity: methods for determining the focus of the SIRTF telescope in space without a focus slew", in *IR Space Telescopes and Instruments*, ed. J. C. Mather, Proc. SPIE, 4850, 428, 2002
2. D. B Gallagher, "The development and mission of the Spitzer Space Telescope" ", in *Astronomical Telescopes and Instrumentation*, Proc. SPIE , [5487-01]**,** in press, 2004
3. T. L. Roellig, M. Werner, D. Gallagher, W. Irace, G. G. Fazio, J. Houck, G. Rieke, R. Wilson, "On-orbit performance of the Spitzer Space Telescope" ", in *Astronomical Telescopes and Instrumentation*, Proc. SPIE , [5487-03]**,** in press, 2004
4. J. L. Hora, G. G. Fazio, L. E. Allen, M. L. N. Ashby, P. Barmby, L. K. Deutsch, J.-S. Huang, M. Marengo, S. T. Megeath, G. J. Melnick, M. A. Pahre, B. M. Patten, H. A. Smith, Z. Wang, S. P. Willner, W. F. Hoffmann, J. L. Pipher, W. J. Forrest, C. W. McMurty, C. R. McCreight, M. E. McKelvey, R. E. McMurray, S. H. Moseley, R. G. Arendt, J. E. Mentzell, C. Trout-Marx, D. Fixen, E. V. Tollestrup, P. Eisenhardt, D. Stern, V. Gorjian, B. Bhattacharya, S. Carey, W. J. Glaccum, M. Lacy, P. J. Lowrance, S. Laine, B. O. Nelson, W. T. Reach, J. R. Stauffer, J. A. Surace, G. Wilson, E. L. Wright, "In-flight performance of the Infrared Array Camera (IRAC) for the Spitzer Space Telescope", in *Astronomical Telescopes and Instrumentation*, Proc. SPIE , [5487-06], in press, 2004
5. G. G. Fazio, J. L. Hora, L. E. Allen, M. L. N. Ashby, P. Barmby, L. K., Deutsch, J.-S. Huang, S. Kleiner, M. Marengo, S. T. Megeath, G. J. Melnick, M. A. Pahre, B. M. Patten, J. Polizotti, H. A. Smith, R. S. Taylor, Z., Wang, S. P. Willner, W. F. Hoffmann, J. L. Pipher, W. J. Forrest, C. W., McMurty, C. R. McCreight, M. E. McKelvey, R. E. McMurray, D. G. Koch, S. H., Moseley, R. G. Arendt, J. E. Mentzell, C. Trout-Marx, P. Losch, P. Mayman, W. Eichhorn, D. Krebs, M. Jhabvala, D. Y. Gezari, D. J. Fixsen, J. Flores, K. Shakoorzadeh, R. Jungo, C. Hakun, L. Workman, G. Karpati, R. Kichak, R., Whitley, S. Mann, E. V Tollestrup, P. Eisenhardt, D. Stern, V. Gorjian, B., Bhattacharya, S. Carey, B. O. Nelson, W. J. Glaccum, M. Lacy, P. J., Lowrance, S. Laine, W. T. Reach, J. A. Stauer, J. A. Surace, G. Wilson, E., L.Wright, A. Homan, G. Domingo, M. Cohen, "The Infrared Array Camera (IRAC) for the Spitzer Space Telescope", APJ, *accepted for publication*
6. M. Lacy, R. G. Arendt, M. L. N. Ashby, P. Eisenhardt, G. G. Fazio, W. J. Glaccum, J. L. Hora, S. T. Megeath, W. T. Reach, J. A. Surace, Z. Wang, S. P. Willner, L. E. Allen, P. Barmby, B. Bhattacharya, S. J. Carey, L. K. Deutsch, W. F. Hoffmann, J. Huang, M. Im, S. Laine, P. J. Lowrance, M. Marengo, S. H. Moseley, B. O. Nelson, M. A. Pahre, B. M. Patten, J. Stauffer, D. Stern, C. Trout-Marx, G. Wilson, "Observing with the infrared array camera (IRAC) on the Spitzer Space Telescope", in *Astronomical Telescopes and Instrumentation*, Proc. SPIE, [5487-90], in press, 2004
7. R. D. Gehrz, E. A. Romana, W. F. Hoffmann, J. P. Schwenker, J. E. Mentzell, J. L. Hora, P. Eisenhardt, B. R. Brandl, L. Armus, K. R. Stapelfeldt, D. Hines, A. K. Mainzer, E. T. Young, and D. G. Elliott, "The state of the focus and image quality of the Spitzer Space Telescope as measured in orbit", in *Astronomical Telescopes and Instrumentation*, Proc. SPIE , [5487-86]**,** in press, 2004
8. J. P. Schwenker, B. R. Brandl, W. L. Burmester, J. L. Hora, A. K. Mainzer, J. E. Mentzell, J. E. VanCleve, "SIRTF-CTA Optical Performance Test Results", in *IR Space Telescopes and Instruments*, ed. J. C. Mather, Proc. SPIE, 4850, 30, 2002
9. J. P. Schwenker, B. R. Brandl, W. F. Hoffmann, J. L. Hora, A. K. Mainzer, P. C. Quigley, J. E. VanCleve, "SIRTF-CTA Optical Performance Test", in *IR Space Telescopes and Instruments*, ed. J. C. Mather, Proc. SPIE, 4850, , 2002
10. C. J. Burrows, "Hubble Space Telescope optics – problems and solutions:, Proc. SPIE, 1494, 528, 1991
11. E. L. Wright, "On using a space telescope to detect faint galaxies", *PASP*, **97**, pp 451-453, 1985